ISSN 0018-151X, High Temperature, 2017, Vol. 55, No. 4, pp. 573–578. © Pleiades Publishing, Ltd., 2017.
Original Russian Text © A.F. Polyakov, 2017, published in Teplofizika Vysokikh Temperatur, 2017, Vol. 55, No. 4, pp. 589–595.

HEAT AND MASS TRANSFER AND PHYSICAL GASDYNAMICS

Implementation of Stable Thermal Stratification in Tubes and Near-Wall Turbulence Suppression

A. F. Polyakov

Joint Institute for High Temperatures, Russian Academy of Sciences, Moscow, 127412 Russia

e-mail: paf2003@mail.ru

Received March 20, 2016

Abstract—An analysis and generalization are performed of experimental data on near-wall turbulence damping under the influence of stable thermal stratification of density in vertical and horizontal tubes with rectangular and circular cross-sections.

DOI: 10.1134/S0018151X17040186

INTRODUCTION

We consider three variants of implementation of stable thermal stratification (SRS) at a turbulent flow of uniform fluid in tubes: (1) in the limits of full laminarization of the flow in a horizontal flat channel heated from above; (2) restricted by a range of relatively weak lifting forces before the beginning of the influence of free convection at an ascending fluid flow in vertical heated tubes; and (3) at strong thermogravity (lifting force in nonisothermal conditions) influence on the local SRS formation near the upper generatrix in horizontal heated circular tubes. In all three cases, the walls are heated by an electric current; that is, the second kind boundary condition, $q_w = \text{const}$, is assigned. We consider the steady-state flows far from the surface streamline beginning at the moderate Reynolds numbers ($\text{Re} = \bar{u}d/\nu < 5\times10^4$). Here, $\bar{u}$ is the averaged velocity over the fluid flow cross-section; d, the internal tube diameter; ν, the kinematic viscosity coefficient.

In normal (unperturbed) conditions, the wall turbulence state is characterized by universal parameters (discussed, in particular, in [1]): the value and the location of the pulsation intensity of the longitudinal velocity component and the density of the turbulent energy generation. The dimensionless parameter of the turbulence anisotropy [2] is one more generalized characteristic of the turbulent flow. All the available works on the study of pulsation characteristics present data on the pulsation intensity of the longitudinal velocity component—the most accessible in the measurements. Data on other components and their correlations are scantier. This fact is naturally reflected in the content of the present paper.

After presentation of the initial data for the unperturbed flows, we analyze the variation of the above indices under the SRS application on the wall flows, that is, on the wall turbulence suppression resulting in a decrease of the friction drag and of the heat transfer in the above-mentioned cases. The last one is an urgent engineering problem.

Peculiarities of the density distribution of the wall generation of turbulence are considered in [3]; there, the data are presented for the undisturbed wall flows of the uniform monophase fluid as well as for the flows undergoing the various impacts causing the turbulence damping, including the SRS. In the present work, we do not present the results on the turbulence generation density discussed in [3]. Yet, here, they are supplemented with the experimental data for the case of strong SRS influence at the lifting air movement in the heated tube – these data are of interest when compared with data on the intensity of pulsations of the longitudinal velocity component.

AVERAGED CHARACTERISTICS OF NEAR-WALL TURBULENCE IN UNDISTURBED FLOWS

Intensity of the Longitudinal Velocity Pulsations

In [1], a conclusion was made on the universality of the intensity distribution of the longitudinal velocity pulsations in the universal wall coordinates, $\sigma^+_{u0} = \sqrt{\langle u'^2\rangle_0}/v_*, y^+$ with the maximal value $\sigma^{+\max}_{u0} = 2.5 - 2.7$ taking place in the buffer layer domain at $y^+ \cong 14$. Here, $y^+ = yv_*/\nu$ is the normal (to the wall) coordinate; $v_* = \sqrt{\tau_w/\rho}$, the dynamic velocity (the friction velocity); τ_w, the friction strength on the wall; ρ, the density. The "+" superscript at σ_u means dimensionless state as against v_*, and the 0 subscript corresponds to the unperturbed flow.

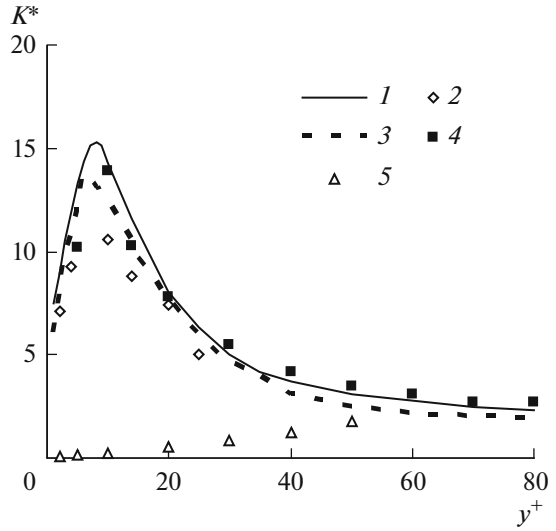

Fig. 1. Distribution of the turbulence anisotropy parameter: (*1*) flat channel [2]; (*2*) flat channel, $\mathrm{Re} \cong 2\times10^4$ [7]; (*3*) circular tube, $\mathrm{Re} = 10^4$ [5]; (*4*) circular tube, $\mathrm{Re} = 6\times10^3$ [1]; (*5*) horizontal circular tube, $\varphi = 0$, $\mathrm{Re} = 1.2\times10^4$, $\mathrm{Gr}/\mathrm{Gr}_0 = 110$ [8, 9].

The concept of the universality of the longitudinal pulsation intensity distribution in the universal coordinates immediately near the wall ($y^+ < 40$) at the given values of their maximal value is totally confirmed by experimental data [4] for the circular cross-section tube within the Reynolds numbers range $2520 \le \mathrm{Re} < 5\times10^4$. The curve for the normal conditions will be presented below when discussing the SRS influence. The results of the direct numerical modeling (DNM) [1, 5] coincide with the data [4]. The experimental data [6] obtained at $\mathrm{Re} = 4.2\times10^4$ correspond to results [4]. Note that the experimental data [4] on the intensity of the normal (to the wall) pulsations within the above stated Reynolds numbers range at $y^+ > 10$ very heavily split depending on the Re and their maximal values are within the range of 0.7 to 1.1 at their coordinate variation from $y^+ = 40$ to $y^+ = 200$.

Turbulence Anisotropy Parameter

The dimensionless energy parameter of the turbulence anisotropy is governed by combination of the dispersions of the velocity component pulsations [2]:

$$K^* = \frac{2\sigma_u^2}{\sigma_v^2 + \sigma_w^2}, \qquad (1)$$

where σ_u^2, σ_v^2, σ_w^2 are the pulsation dispersion components of the longitudinal, normal, and tangential velocities, respectively. At the isotropic turbulence, the anisotropy parameter $K^* = 1$.

Figure 1 (curve and symbols *1–4*) shows the K_0^* distributions in the wall coordinates for the standard conditions. Here, we engaged the results [1, 2, 5, 7] where the data are obtained on the turbulent pulsation intensities over all three coordinates. The curve *1* plotted according to the experimental data for the flat channel at the low Reynolds numbers is taken from [2]. Based on the results of [2], we make a conclusion that, within the range $2 \le y^+ \le 30$–35, at the K_0^* values more than five but less than the maximal value (at 15), the vortex structure of turbulence is implemented. The DNM results [1] for the circular tube at $\mathrm{Re} = 6\times10^3$ (dots *4*) are the nearest to the curve *1* of the presented data for the unperturbed flows. With the Reynolds number increase, the local K_0^* values near the maximum somewhat decrease (*2* and *3* in Fig. 1). The attempt to apply the $\sigma_w^2 = (\sigma_u^2 + \sigma_v^2)/2$ approximation for the works where the σ_w^2 value was not measured shows total inconsistency of such approach of the K^* determination. Here, for the data shown in Fig. 1, the $\tilde{K}_0^*$ value within the whole y^+ range turns to be less than 4.

REGIMES WITH SRS INFLUENCE

To demonstrate the degrees of influence of the considered SRS effects, Fig. 2 shows two lines, *1* and *2* (taken from [4]) for the longitudinal velocity pulsations. The experimental data [7] (dots *3*) in fact confirm the results [4].

Horizontal Flat Channel

In JIHT, RAS, we experimentally investigated the air turbulent flow under the conditions of stable thermal stratification in the horizontal channel with heated upper wall [10]. We performed the measurements by means of thermoanemometer with temperature compensation. In the case of stable stratification in the horizontal fluid flow, implementation is possible of in fact total flow relaminarization – it might be estimated as $\mathrm{Gr}_{2h} = g\beta q_w (2h)^4/(\lambda\nu^2) > 8\mathrm{Re}_{2h}^2$ ($\mathrm{Re}_{2h} = \bar{u}2h/\nu$, h—the channel height) [11]. In [11], we used the approaches developed in the theory of the temperature-stratified medium applied to the problems of geophysics [12]. Fig. 2 shows the experimental data [10] at $\mathrm{Re}_{2h} = 6400$ for the neutral ($\mathrm{Gr}_{2h} = 0$) stratification (dots *4*) and for $\mathrm{Re}_{2h} = 6000$ for the strong stable ($\mathrm{Gr}_{2h} = 10^8$, $\mathrm{Gr}_{2h}/\mathrm{Gr}_{2h0} = 55$) stratification (dots *5*). Here, Gr_{2h0} is the beginning of the thermogravity influence characterized by the 1% decrease of the heat transfer [11]. The maximal value and the location of the $\sigma_{u0}^{\max}$ for the neutral stratification somewhat differ from the generalized curve *1*: it is possibly related with the low Reynolds number and insufficient channel

width, 1 : 4, because, for the reliable analogy with the flat channel, the recommended relation is more than 1 : 6 [13]. The dots *5* demonstrate strong decrease of the turbulent pulsation intensity. According to the estimate of total relaminarization, $\mathrm{Gr}_{2h}^{\mathrm{lam}} = 8\,\mathrm{Re}^2 = 2.9\times10^8$, this is an evidence of approaching of the considered regime with $\mathrm{Gr}_{2h} = 10^8$ to the stated boundary. The friction coefficient decreases by the value of $c_f/c_{f0} \cong 0.6$ [11].

Vertical Tube

Turbulence damping at the ascending air movement in the heated vertical tube is implemented only at the initial stage of impact of the stable thermal stratification ($dT/dx > 0$); with the thermal loading increase, free-convective turbulent flow of the fluid begins to prevail thus causing an increase of turbulent pulsations, frictional drag, and heat transfer [11]. The "free convection regime" is the extreme regime in that situation.

We obtained the experimental data [14, 15] at the bottom-up air flow in the vertical heated tube using the two-coordinate laser Doppler anemometer. In [16], we show that at the initial stage of the thermogravity influence, the heat transfer decrease is related with the turbulence suppression. Here, the extreme Grashof number, Gr_0, at which the lifting forces still do not influence essentially on the heat transfer at the stimulated flow [16] is characterized by 1% deviation of the Nusselt number from its value without the thermogravity influence at the Prandtl numbers $\mathrm{Pr} = \rho c_p \nu/\lambda = 0.6$–$200$ and is defined by the following dependence:

$$\mathrm{Gr}_0 = 9\times10^{-5}\,\mathrm{Pr}^{1.15}\,\mathrm{Re}^{2.75}.$$

Here, $\mathrm{Gr} = g\beta q_w d^4/(\lambda\nu^2)$ for the boundary condition $q_w = \mathrm{const}$; $g = 9.81$ m/s^2, the acceleration of gravity; λ, the thermal conductivity coefficient; and $\beta = -\frac{1}{\rho}\left(\frac{\partial\rho}{\partial T}\right)_p$, the volume expansion coefficient of the fluid.

Figure 2 also shows (dots *6*) the σ_u^+ distribution at $\mathrm{Re} = 9\times10^3$ and relatively weak SRS influence, that is, at $\mathrm{Gr}/\mathrm{Gr}_0 = 4.4$. In that case, $\sigma_u^{+\max}$ already strongly decreases to the value of 1.6 at in fact the same coordinate, $y^+_{\max} \cong 14$, as in the undisturbed flow cases. With the increase of the SRS influence, both the maximal value and the coordinates of $\sigma_u^{+\max}$ vary essentially (see dots *7*–*9* for $\mathrm{Re} = 5100$ at $\mathrm{Gr}/\mathrm{Gr}_0$ and at 9.6, 11.7, 16, respectively). Thus, almost total damping of turbulence took place near the wall and its maximal value shifted to the tube center. Then, the SRS conditions get broken and intensive turbulent free convection develops [9].

The case of extreme damping of the wall turbulence at $\mathrm{Gr}/\mathrm{Gr}_0 = 16$ is of special interest. According to the

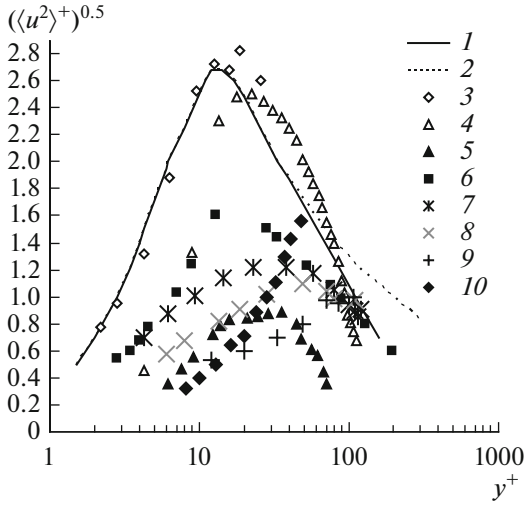

Fig. 2. Intensity of the longitudinal velocity pulsation in the universal wall coordinates: (*1*) Re = 5540 [4]; (*2*) 10300 [4]; (*3*) 2×10^4 [7]; (*4*) 6400, $\mathrm{Gr} < \mathrm{Gr}_0$ [10]; (*5*) 6000, $\mathrm{Gr}/\mathrm{Gr}_0 = 55$ [10]; (*6*) 9000, 4.4 [14, 15]; (*7*) 5100, 9.6 [14, 15]; (*8*) 11.7 [14, 15]; (*9*) 16 [14, 15]; (*10*) $\mathrm{Re} = 1.2\times10^4$, $\mathrm{Gr}/\mathrm{Gr}_0 = 110$ [8, 9, 21].

experimental data available, one might determine the turbulence generation density for this case neglecting the effect of the free convection influence, that is

$$Gt = -\langle u'v'\rangle^+ \frac{du^+}{dy^+}. \qquad (2)$$

In [3], we did not consider that case.

Figure 2 also presents our results [14, 15] being the evidence of essential σ_u^+ decrease in the regime with the parameters $\mathrm{Pr} = 0.7$, $\mathrm{Re} = 5100$, $\mathrm{Gr} = 9\times10^6$ ($\mathrm{Gr}_0 = 9.4\times10^5$, $\mathrm{Gr}/\mathrm{Gr}_0 = 9.6$) (dots *7*). The data on the *Gt* for this case are presented in [3] and in the Table. The maximal values of σ_u^+ and *Gt* decrease by 2.2 and 5 times, respectively, remaining in fact at the same coordinates as in the case of unperturbed flows.

For the regime of maximal suppression of the wall turbulence ($\mathrm{Pr} = 0.7$, $\mathrm{Re} = 5100$, $\mathrm{Gr} = 1.5\times10^7$, $\mathrm{Gr}/\mathrm{Gr}_0 = 16$), the velocity profile is approximated by the dependence

$$u^+ = 17.5[1 + 0.424(1 - y^+/170) - 1.424(1 - y^+/170)^{7.42}].$$

The measured $\langle u'v'\rangle^+$ values for this regime [14, 15] are presented in the Table 1 as well as the results of the *Gt* calculation according to (2).

Character of the $Gt(y^+)$ distribution at $\mathrm{Gr}/\mathrm{Gr}_0 = 9.6$ and $\mathrm{Gr}/\mathrm{Gr}_0 = 16$ is in fact the same; yet, their abso-

Table 1. Distributions of the Reynolds strength in the wall domain at $\mathrm{Gr}/\mathrm{Gr}_0 = 16$ and of the turbulence generation densities in the vertical heated tube

y^+	10	15	27	34	42
$-\langle u'v'\rangle^+$	0.0066	0.009	0.0105	0.0121	0.0145
$Gt\ (\mathrm{Gr}/\mathrm{Gr}_0 = 16)$	0.004	0.0047	0.003	0.0023	0.0016
$Gt\ (\mathrm{Gr}/\mathrm{Gr}_0 = 9.6)$	0.030	0.048	0.036	0.025	0.017
$Gt\ (\mathrm{Gr} < \mathrm{Gr}_0)$	0.22	0.23	0.20	0.12	0.08

lute values differ by the order of magnitude. Here, the locations of the maximal Gt values coincide.

In the case of the extreme suppression of the wall ($y^+ < 50$) turbulence at $\mathrm{Gr}/\mathrm{Gr}_0 = 16$, the degree of decrease of the maximal σ_u^+ and Gt values differs essentially from the initial data for the unperturbed flows. If the σ_u^+ maximum (Fig. 2, dots *9*) decreases 2.7 times, that is, by almost the same value as in the $\mathrm{Gr}/\mathrm{Gr}_0 = 9.6$ regime, but with strong shift of the maximum location up to the wall domain boundary, then the Gt decreases by almost 50 times with, in fact, total conservation of the maximum location. Thus, the obtained results for $\mathrm{Gr}/\mathrm{Gr}_0 = 16$ differ essentially from those for $\mathrm{Gr}/\mathrm{Gr}_0 = 9.6$. This is evidently caused by the already developed influence of the free convection.

In both considered cases, the SRS at the strong flow laminarization in the horizontal flat channel ($\mathrm{Gr}/\mathrm{Gr}_0 = 55$) and at the extreme degree of the wall ($y^+ < 50$) turbulence damping in the vertical heated tube ($\mathrm{Gr}/\mathrm{Gr}_0 = 16$) about the same degree of intensity damping of the longitudinal velocity pulsation takes place (Fig. 2, dots *5* and *9*, respectively).

Along with study of the turbulent mixed convection, in the JIHT, RAS, at the same experimental base, we investigated the uplifting turbulent flow of the air with the solid particles in the vertical tube. We gave special attention to the regimes with turbulence damping [17, 18]. We performed the experiments at Re = 25600 with spherical aluminum oxide and glass monoparticles. The strongest turbulence damping not near the wall but in the middle of the tube is the case peculiarity, in contrast to the SRS. In particular, use of the glass particles ($d_p = 50$ μm) results in the σ_u^+ decrease at $R = 0.8$ from $\sigma_{u0}^+ \cong 1.9$ to $\sigma_u^+ \cong 1.1$, whereas, at the nearest measurement point to the wall, at $R = 0.95$, there is no σ_u^+ variation, that is, $\sigma_u^+ \cong \sigma_{u0}^+$.

Yet, the dust-laden air flow with lighter particles gives results qualitatively similar to the considered SRS case. In the review [19], along with the data [17], the experimental results [20] are presented for the ascending air movement, with lighter plastic particles ($d_p = 200$ μm, $\rho_p = 1000$ kg/m^3), in the tube.

In the last case, at the nearest distance from the wall ($R = 0.93$), at the mass concentration of the disperse phase, $M = 3.2$, the intensity of the longitudinal pulsations of the bearing phase—air—decreased essentially $(\sigma_u/\sigma_{u0})\big|_{R=0.93} \cong 1.5$, whereas, at the axis, it did not in fact vary $(\sigma_u/\sigma_{u0})\big|_{R=0} \cong 1$.

Thus, at the ascending turbulent air flow in the vertical tube, a qualitative analogy is seen between the SRS at the low thermal loading with the mixed (in the limit—free) convection at high thermal loading and the weakly dust-laden flow when the flow takes off the light disperse phase particles with the next stage when the hard particles "impose" their dominating influence on the pulsation structure of the continuous medium.

SRS in Horizontal Tube and Analysis of the Turbulence Energy

The local SRS development in the upper part of the heated horizontal tube [8, 9] differs essentially from the two above-considered cases.

Presence of the radial temperature gradient in the horizontal circular channel, both in laminar and in turbulent fluid flow, results in development of the secondary free-convective flows. With the thermal loading increase, along with development of the free-convective flows, the thermogravity forces begin to influence on the wall turbulence: at the local SRS, near the upper generatrix, the turbulent transfer decreases, causing a variation of the secondary flow pattern.

When studying the local SRS near the upper generatrix of the horizontal tube, we performed direct measurements of distributions of the velocity components, the intensity of pulsations of the longitudinal velocity component, $\sigma_u^+ = \sqrt{\langle u'^2\rangle}/v_*$, the specific turbulence energy, $E = (\sigma_u^2 + \sigma_v^2 + \sigma_w^2)/2$, and the local frictions at the wall. To measure the velocity vector components and the turbulence energy, we applied the specially developed measurement technique by means of the rotary thermo-anemometric probe with temperature compensation.

In the present work, we paid primary attention to the strong SRS manifestation near the upper generatrix at $\mathrm{Re} = 1.2\times10^4$, $\mathrm{Gr}/\mathrm{Gr}_0 = 110$. For the analysis of the presented experimental data in the wall coordinates, of principal importance are the performed direct measurements of the distributions of the friction strengths at the wall, τ_w, over the circle [21]. Within the range of $-15° \le \varphi \le 15°$, the τ_w value is 0.0035 N/m^2, that is, by about three times less than the frictional drag at the isothermal flow. The angular coordinate, φ, is counted from the upper generatrix.

In the immediate vicinity of the upper generatrix of the horizontal tube, the conditions correspond to the SRS conditions near the upper heated wall of the horizontal flat channel [10]. In that connection, in Fig. 2, we juxtapose the data on $\sigma_u^+(y^+)$ at the strong SRS influence. Here, near the wall ($y^+ < 40$), the data on σ_u^+ at the strong SRS influence ($\mathrm{Gr}/\mathrm{Gr}_0 = 55$) in the flat channel (Fig. 2, dots *5*) and $\mathrm{Gr}/\mathrm{Gr}_0 = 110$ (Fig. 2, dots *10*) in the circular tube ($\varphi = 0$) are close to each other. Here, we observe an extremely high degree of the turbulence suppression as against the isothermal flow (line *1*). This comparison clearly illustrates the cause of the wall turbulence suppression in the horizontal heated tube near the upper generatrix. At moving away from the wall, use of the wall coordinates is not justified because of essential τ_w variation over the tube perimeter.

The σ_u gives the dominating contribution into the turbulence energy; the plot in the universal wall coordinates, $E^+(y^+)$, (Fig. 3) is qualitatively similar to the plot for $\sigma_u^+(y^+)$ (Fig. 2). Within the $\varphi = 0$, $y^+ < 50$ domain (Fig. 3), strong damping of the turbulence energy, E^+ (dots *3*), is observed similar to the $\sigma_u^+(y^+)$ behavior. Then, within the $\varphi = \pi/2$, $y^+ < 30$ domain, the E^+ value (dots *4*) is essentially higher than E_0^+ (line *1*). If one corresponds $E^+\big|_{\varphi=\pi/2}$ not to $\tau_w\big|_{\varphi=\pi/2}$ but to $\overline{\tau}_w$, then the dots at $y^+ > 30$ will naturally rise; yet, such variations are evidently unpractical.

The results of the turbulence measurements in the SRS conditions (considered in the two preceding sections) give no opportunity to determine the value of the energy parameter, K^*. The measured σ_u^+ and E_0^+ values in the considered case make it possible to determine the anisotropy parameter: in the wall coordinates, according to the definition (1), it is written as follows:

$$K^* = \frac{2\sigma_u^{+2}}{2E^+ - \sigma_u^{+2}}. \qquad (3)$$

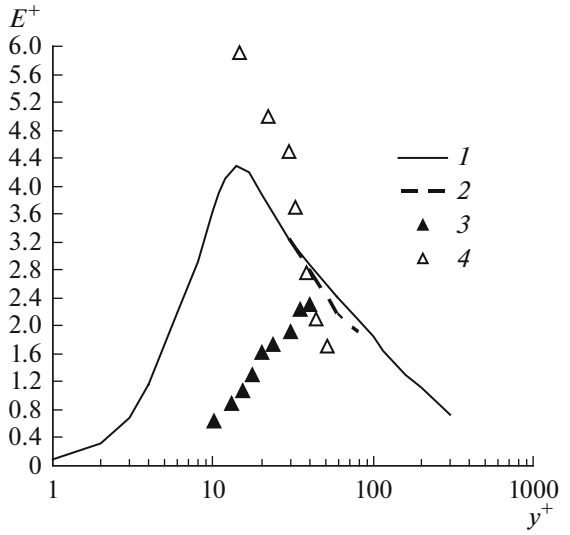

Fig. 3. Turbulence energy distributions in the universal wall coordinates: (*1*) E_0^+, $\mathrm{Re} = 10^4$ [5]; (*2*) Re = 6000 [1]; (*3*) $\mathrm{Re} = 1.2\times10^4$, $\mathrm{Gr}/\mathrm{Gr}_0 = 110$, $\varphi = 0$ [8, 9, 21]; (*4*) $\varphi = \pi/2$.

Note that, at the isotropic turbulence, $E^+ = \frac{3}{2}\sigma_u^{+2}$.

In Fig. 1, in the comparison with the data for the undisturbed flows, the results are presented of calculations [18, 19] according to (3) with use of the experimental σ_u^{+2} and E^+ values at $\varphi = 0$ for the case of strong influence of the local SRS ($\mathrm{Re} = 1.2\times10^4$, $\mathrm{Gr}/\mathrm{Gr}_0 = 110$).

The turbulence anisotropy parameter, K^*, not only is evidence of the turbulence presence in the flow but extracts the particular ranges characterizing its structure. There is no marked above vortex turbulent structure within the $2 \le y^+ \le 30$–35 range at the $K_0^* = 5$–15 values, naturally, at the $K_0^* = 0.05$–1.0 values within the above stated y^+ range (Fig. 1, dots *5*). The K^* parameter, beginning from the turbulence damping state near the wall, passes, at $y^+ = 35$, the "isotropic turbulence" state ($K^* = 1$). Then, it approaches the values typical for the wall turbulence far from the wall.

CONCLUSIONS

For the turbulent flows of the monophase medium in the heated tubes, we analyzed the near-wall turbulence characteristics in the conditions of implementation of the stable thermal stratification of the density. We considered the following characteristics: intensity of the longitudinal velocity pulsations, turbulence generation density, turbulence energy, energy parameter of the turbulence anisotropy. The data are jointly

presented on these characteristics variation in the different conditions of implementation of the stable thermal stratification in the heated tubes: in the horizontal flat channel with the heated upper wall; in the vertical tube with the ascending air flow under moderate thermal loadings; and in the circular cross-section horizontal tube under intensive heating. Thus, the effect of the near-wall turbulence suppression by means of impact of the stable thermal stratification takes place in the very different restricted conditions and, hence, requires special attention in the engineering practice.

REFERENCES

1. Nikitin, N.V., *Fluid Dyn.*, 1996, vol. 31, no. 3, p. 361.
2. Lee, M.J., Kim, J., and Moin, P., *J. Fluid Mech.*, 1990, vol. 216, p. 561.
3. Polyakov, A.F., *High Temp.*, 2016, vol. 54, no. 2, p. 257.
4. Polyakov, A.F., Shindin, S.A., and Komarov, P.L., in *Turbulentnyi teploobmen pri smeshannoi konvektsii v vertikal'nykh trubakh* (Turbulent Heat Transfer in Mixed Convection in Vertical Pipes), Moscow: Inst. Vys. Temp., Akad. Nauk SSSR, 1989, p. 25.
5. Nikitin, N.V., *Fluid Dyn.*, 2009, vol. 44, no. 5, p. 652.
6. Bremhorst, K. and Walker, T.B., *J. Fluid Mech.*, 1973, vol. 61, p. 173.
7. Khabakhpasheva, E.M. and Mikhailova, E.S., in *Eksperimental'noe issledovanie struktury pristennoi turbulentnosti i vyazkogo podsloya* (Experimental Study of the Structure of Wall Turbulence and a Viscous Sublayer), Kutateladze, S.S., Ed., Novosibirsk: Sib. Otd. Akad. Nauk SSSR, 1976, p. 33.
8. Petukhov, B.S., Polyakov, A.F., Troitskii, V.V., and Shekhter, Yu.L., *Dokl. Akad. Nauk SSSR*, 1977, vol. 236, no. 4, p. 820.
9. Petukhov, B.S., Polyakov, A.F., Troitskii, V.V., and Shekhter, Yu.L., in *Teploobmen-1978. Sovetskie issledovaniya. Sbornik* (Heat Transfer-1978. Soviet Research: Collection of Papers), Moscow: Nauka, 1980, p. 135.
10. Petukhov, B.S., Polyakov, A.F., and Tsypulev, Yu.V., in *Turbulentnye sdvigovye techeniya 2. Sbornik* (Turbulent Shear Flows 2: Collection of Papers), Moscow: Mashinostroenie, 1983, p. 166.
11. Petukhov, B.S. and Polyakov, A.F., *Teploobmen pri smeshannoi turbulentnoi konvektsii* (Heat Transfer in Mixed Turbulent Convection), Moscow: Nauka, 1986.
12. Monin, A.S. and Yaglom, A.M., *Statisticheskaya gidromekhanika* (Statistical Hydromechanics), Moscow: Nauka, 1965, part 1.
13. Din, R.B., *Tekh. Obsluzh. Remont*, 1978, vol. 100, no. 2, p. 189.
14. Polyakov, A.F. and Shindin, S.A., *Teplofiz. Vys. Temp.*, 1986, vol. 24, no. 5, p. 1031.
15. Polyakov, A.F. and Shindin, S.A., *Int. J. Heat Mass Transfer*, 1988, vol. 31, no. 5, p. 987.
16. Polyakov, A.F., *Teplofiz. Vys. Temp.*, 1973, vol. 11, no. 1, p. 106.
17. Varaksin, A.Yu., Polezhaev, Yu.V., and Polyakov, A.F., *High Temp.*, 1998, vol. 36, no. 5, p. 744.
18. Varaksin, A.Yu. and Zaichik, L.I., *High Temp.*, 1998, vol. 36, no. 6, p. 983.
19. Varaksin, A.Yu., *High Temp.*, 2015, vol. 53, no. 3, p. 423.
20. Tsuji, Y., Morikawa, Y., and Shiomi, H., *J. Fluid Mech.*, 1984, vol. 139, p. 417.
21. Petukhov, B.S., Polyakov, A.F., Troitskii, V.V., and Shekhter, Yu.L., *Teplofiz. Vys. Temp.*, 1982, vol. 20, no. 3, p. 490.

Translated by I. Dikhter